



OPEN ACCESS

EDITED BY

Shouxun Ji,
Brunel University London,
United Kingdom

REVIEWED BY

Hui Guo,
Shanghai University of Engineering
Sciences, China
Guoshuang Shui,
Beijing Jiaotong University, China

*CORRESPONDENCE

Xiaoli Zhu,
✉ zhuxiaoli40@163.com

RECEIVED 10 July 2023

ACCEPTED 12 September 2023

PUBLISHED 28 September 2023

CITATION

Ling Y, Zhu X and Song L (2023),
Application of periodic structural wave
impeding block for vibration isolation in
foundation.
Front. Mater. 10:1256098.
doi: 10.3389/fmats.2023.1256098

COPYRIGHT

© 2023 Ling, Zhu and Song. This is an
open-access article distributed under the
terms of the [Creative Commons
Attribution License \(CC BY\)](#). The use,
distribution or reproduction in other
forums is permitted, provided the original
author(s) and the copyright owner(s) are
credited and that the original publication
in this journal is cited, in accordance with
accepted academic practice. No use,
distribution or reproduction is permitted
which does not comply with these terms.

RETRACTED: Application of periodic structural wave impeding block for vibration isolation in foundation

Yongqiang Ling^{1,2,3}, Xiaoli Zhu^{3*} and Lei Song^{1,2}

¹State Key Laboratory of Intelligent Construction and Healthy Operation and Maintenance of Deep Underground Engineering, Xuzhou, Jiangsu, China, ²Yunlong Lake Laboratory of Deep Underground Science and Engineering, Xuzhou, Jiangsu, China, ³School of Architecture and Engineering, Shanghai Zhong Qiao Vocational and Technical University, Shanghai, China

The wave impeding board (WIB) is frequently integrated beneath dynamic machinery, tracks, and subgrades to counteract vibrations emanating from artificial sources. However, conventional WIBs have exhibited a limited isolation frequency band due to their dependence on the soil cut-off frequency of soil. Furthermore, the vibration sources typically encompass intricate frequency components spanning low, medium, and high frequencies. To overcome the technical limitations of WIBs relying on the cut-off frequency of soil, a new periodic structural wave impeding board (PSWIB) is proposed based on the principles of phononic crystals. Theoretical and numerical analyses demonstrate that PSWIB exhibits bandgap characteristics, with the attenuation range achieved by finite periodic structures aligning with the bandgap of an infinite PSWIB. Maximum amplitude reductions of 47 dB and 65 dB are achieved within the vibration attenuation range. Compared to traditional WIB, PSWIB surpasses the constraints imposed by the cut-off frequency of soil and allow for the design of constituent parameters based on the characteristics of the vibration source, enabling effective isolation of the target frequency vibrations.

KEYWORDS

periodic structure, wave impedance board, band gap, attenuation domain, foundation

1 Introduction

Wave impeding board (WIB), commonly deployed in the subgrade soil, is widely used as vibration isolation barriers to mitigate vibrations generated by artificial sources (Takemiya and Fujiwara, 1994; Ma et al., 2022). The principle of the WIB is to modify the wave propagation regime of the ground by introducing an artificial horizontal stiffened layer. The wave transmission regime in the ground depends on the relationship between the excitation frequency of the source and the cut-off frequency of the overlaying soil above the WIB. When the exciting frequency is higher than the cut-off frequency, wave will transmit. Otherwise, wave transmission will be prevented (Chow et al., 1991; Schmid et al., 1992; Chen et al., 2022).

Ever since the inception of WIBs by Schmid et al. (1992), extensive research has been conducted by scholars. Schmid et al. (1992), as well as Takemiya et al. (2002), Takemiya, (2003), Takemiya, (2004), have analyzed the vibration isolation and damping performance of WIBs, indicating their effectiveness as reliable vibration isolation measures. Additionally, Takemiya et al. proposed a honeycomb-shaped WIB and conducted on-site experiments, demonstrating its superior vibration isolation performance. Peplow et al. (1999) employing the boundary integral equation method, delved into the active vibration isolation capability

of a two-dimensional double-layered subgrade WIB, revealing its competence in regulating vibrations within the low-frequency spectrum. Lombaert et al. (2015) also found that WIBs effectively control low-frequency vibrations induced by railway traffic. Çelebi and Göktepe, (2012), using nonlinear 2D finite element analysis, studied the vibration isolation performance of WIBs on ground vibrations caused by railway traffic, discovering that WIBs with lower impedance ratios provide more effective vibration isolation. Thompson et al. (2015) explored the vibration isolation prowess of WIBs buried beneath railway tracks, revealing significant vibration reduction in the 16–50 Hz frequency range. Li et al. (2023a) analyzed the control effect of WIBs on subway vibrations through numerical soft-ware, demonstrating good vibration isolation performance for frequencies between 5 and 15 Hz. Ma et al. (2019) concentrated on the vibration isolation performance of WIBs under moving loads, concluding that these structures exhibit notable vibration control potential within a 10 Hz frequency. Based on the above research, it is evident that WIBs have significant vibration control effects. Gao et al. (2015); Gao et al. (2017) analyzed the relationship between the WIB and the actual ground conditions in terms of laminar characteristics. The results show that setting WIBs in the foundation near the bottom of the vibration source has significant near-field active vibration damping and isolation effects, and the vibration damping and isolation effects of WIBs can be effectively improved by taking measures such as increasing the thickness of WIBs, improving the modulus of elasticity of WIBs, and decreasing the depth of burial of WIBs. In summary, they are limited by the cut-off frequency of the overlying soil layer, exhibiting better vibration isolation only within the low-frequency range with a narrow isolation band (Peplow and Kaynia, 2007; Yan et al., 2020; Atakan et al., 2022; Li et al., 2023b). Thus, their ability to isolate complex source frequencies is greatly restricted, rendering them unable to meet the increasing demands for vibration isolation.

The periodic structure is mostly used in building surface wave vibration isolation, and the research on reducing the vibration generated by artificial vibration sources such as power machines, tracks and underneath the roadbed is still very limited. Considering the limitations of construction, this paper adopts the simplest possible periodic structure to reduce the vibration generated by artificial vibration sources such as power machines, tracks and underneath the roadbed. To enhance the vibration isolation and damping performance of conventional WIBs by overcoming their dependence on the cut-off frequency of the subgrade soil layer and achieving control and isolation of different source frequencies, a new periodic structural WIB (PSWIB) is proposed based on the principles of phononic crystals. The vibration isolation performance of PSWIB is analyzed and compared using both theoretical and numerical calculations.

2 Theory and model calculation of PSWIB

2.1 Basic theory of plane wave expansion method

The calculation of bandgaps for periodic structures using the plane wave expansion method relies on the periodicity of infinite

phononic crystals (Hsu and Wu, 2006). The Lamé constants, density, and other parameters are expanded as Fourier series in reciprocal lattice space. By applying Bloch's theorem and substituting these expansions into the elastic wave equation, the eigenvalue equation can be obtained. Solving the eigenvalue equation yields the bandgaps of the structure.

An ideal two-dimensional phononic crystal consists of periodically distributed cylindrical pillars extending infinitely along the axial direction within a matrix. The two-dimensional lattice plane is usually chosen as the xy plane, and the axial direction is taken as the z -direction. When elastic waves propagate within the xy plane, the displacement in the medium depends only on x and y coordinates and is independent of the z coordinate, i.e., $u(r, t) = u(x, y, t)$. As a result, the governing equations for elastic waves are simplified into the out-of-plane (z -mode) equation for mass displacement and the in-plane (xy -mode) equation for particle displacement.

The vector equation within the plane is given by:

$$\rho(r) \frac{\partial^2 u_x}{\partial t^2} = \frac{\partial}{\partial x} \left[\lambda(r) \left(\frac{\partial u_x}{\partial x} + \frac{\partial u_y}{\partial y} \right) \right] + \frac{\partial}{\partial x} \left[\mu(r) \left(\frac{\partial u_x}{\partial x} - \frac{\partial u_y}{\partial y} \right) \right] + \frac{\partial}{\partial y} \left[\mu(r) \left(\frac{\partial u_x}{\partial y} + \frac{\partial u_y}{\partial x} \right) \right], \quad (1)$$

$$\rho(r) \frac{\partial^2 u_y}{\partial t^2} = \frac{\partial}{\partial y} \left[\lambda(r) \left(\frac{\partial u_x}{\partial x} + \frac{\partial u_y}{\partial y} \right) \right] + \frac{\partial}{\partial x} \left[\mu(r) \left(\frac{\partial u_y}{\partial x} - \frac{\partial u_x}{\partial y} \right) \right] + \frac{\partial}{\partial y} \left[\mu(r) \left(\frac{\partial u_y}{\partial y} + \frac{\partial u_x}{\partial x} \right) \right]. \quad (2)$$

The scalar equation outside the plane is given by:

$$\rho(r) \frac{\partial^2 u_z}{\partial t^2} = \frac{\partial}{\partial x} \left[\mu(r) \left(\frac{\partial u_z}{\partial x} \right) \right] + \frac{\partial}{\partial y} \left[\mu(r) \left(\frac{\partial u_z}{\partial y} \right) \right], \quad (3)$$

where ρ represents the density of the constituent material, λ and μ denote the Lamé constants of the constituent material, r represents the position vector in space, $r = [x, y, z]^T$, u represents the displacement vector, and u_x , u_y , and u_z represent the displacement components in the x , y , and z directions, respectively.

The density ρ and Lamé constants λ and μ are expanded separately as Fourier series:

$$g(r) = \sum_{G'} g(G') e^{iG' \cdot r}, \quad (4)$$

where $g(r)$ represents the physical quantity of density ρ , Lamé constants λ , and μ at any point r . G' is the reciprocal lattice vector, and $g(G')$ is the Fourier expansion coefficient. i denotes the imaginary unit.

According to the Bloch-Floquet theory, the displacement solution can be expressed as follows:

$$u(r, t) = e^{-i\omega t} \sum_{G'} u_k(G') e^{i(k+G') \cdot r}, \quad (5)$$

where k represents the wave vector, ω is Angular frequency. According to the above theoretical method, substituting Eqs 4, 5 into the basic equation of elastic waves (3) can obtain the eigen equation of the z mode:

$$\omega^2 \sum_{G'} \rho (G'' - G') u_{k+G'}^z (G') = \sum \mu (G'' - G') (k + G') \cdot (k + G'') u_k^z (G'), \tag{6}$$

Substituting the basic equations of elastic waves (1) and (2) can obtain the intrinsic equations of xy mode (7) and (8).

$$\begin{aligned} \omega^2 \sum_{G'} \rho (G'' - G') u_{k+G'}^x (G') = & \sum \mu (G'' - G') (k + G') \cdot (k + G'') u_k^x (G') \\ & + \mu (G'' - G') \left((2(k + G')_x (k + G'')_x + (k + G')_y \cdot (k + G'')_y) \right) u_k^y (G') \\ & + \sum_{G'} \left(\lambda (G'' - G') (k + G')_y (k + G'')_x \right) u_k^y (G') \\ & + \mu (G'' - G') (k + G')_x (k + G'')_y u_k^y (G') \end{aligned} \tag{7}$$

$$\begin{aligned} \omega^2 \sum_{G'} \rho (G'' - G') u_{k+G'}^y (G') = & \sum \mu (G'' - G') (k + G')_y \cdot (k + G'')_x \\ & + \mu (G'' - G') \left((2(k + G')_y (k + G'')_y + (k + G')_x \cdot (k + G'')_x) \right) u_k^x (G') \\ & + \sum_{G'} \left(\lambda (G'' - G') (k + G')_x (k + G'')_y \right) u_k^x (G') \\ & + \mu (G'' - G') (k + G')_y (k + G'')_x u_k^x (G') \end{aligned} \tag{8}$$

Eqs 7, 8 are written as matrices in the form of:

$$\begin{aligned} \omega^2 \begin{bmatrix} \sum_{G'} \rho (G'' - G') & 0 \\ 0 & \sum_{G'} \rho (G'' - G') \end{bmatrix} \begin{bmatrix} u^x (k + G') \\ u^y (k + G') \end{bmatrix} \\ = \begin{bmatrix} M_{xx} & M_{xy} \\ M_{yx} & M_{yy} \end{bmatrix} \begin{bmatrix} u^x (k + G') \\ u^y (k + G') \end{bmatrix}, \end{aligned} \tag{9}$$

where $G'' = G' + G$, $i, j, l = x, y, z$.

$$\begin{aligned} M_{ij} = & \sum_{G'} \mu (G'' - G') \sum_j \left[(k + G'')_j (k + G')_j \right] \delta_{ij} \\ & + \sum_{G'} \lambda (G'' - G') (k + G')_i (k + G'')_i \\ & + \sum_{G'} \mu (G'' - G') (k + G')_i (k + G'')_i. \end{aligned} \tag{10}$$

For the computation of the band gaps in the PSWIB, a custom computational program was crafted using Matlab. Taking advantage of the symmetry properties of the periodic structure, the plane wave expansion method was employed to calculate the band gaps of the PSWIB. In this calculation, only the structural unit cell was considered, and the wave vector k was scanned along the irreducible Brillouin zone boundary Γ -X-M- Γ . This approach enabled the determination of the frequency range encompassing the entire band gap of the structure.

2.2 Model and calculation of PSWIB

Based on the periodic nature of the structure, the conventional WIB was transformed into a periodic design. Two arrangements were considered: a square lattice and an intersecting triangular lattice. In both cases, the constituent materials were embedded in two rows along the length direction of the WIB.

Figures 1A, B illustrate the schematic diagrams of the periodic structural wave impeding block with square and triangular arrangements, respectively. Figures 2A, B depict the unit cells for the square lattice arrangement and the hexagonal unit cells for the triangular lattice arrangement. In these figures, the matrix material is denoted as A, and the constituent materials are denoted as B and C, representing the covering layer and filling material, respectively. The parameter a represents the periodicity,

while R and r denote the outer and inner radii of the covering layer, respectively. The matrix material, covering layer, and filling material are composed of concrete, silicone rubber, and powdered clay, respectively. Detailed material parameters are comprehensively documented in Table 1.

Figures 3A, B display the first Brillouin zone corresponding to the square and hexagonal unit cells of the PSWIB, respectively. The shape of the Brillouin zone is dependent on the crystal structure, with the blue region representing the irreducible Brillouin zone. The high-symmetry points on the boundary are denoted as M, Γ , and X. The dimensions of the unit cells are set as $a = 0.3$ m, $R = 0.14$ m, and $r = 0.12$ m. Utilizing the plane wave expansion method, the calculation of bandgaps was executed, and the outcomes are visually presented in Figure 4.

The vibration frequency caused by engineering dynamic machinery and tracks traffic is mainly distributed in the low-frequency position 0–100 Hz (Gao et al., 2015; Thompson et al., 2015), and only the distribution of the bandgap in the vibration frequency range needs to be analyzed in this study. Based on Figures 4A, B, it can be observed that for the periodic structural wave impeding block with square arrangement, the frequency range of the first complete band gap for the x and y mode is 61 Hz–93 Hz, with a gap width of 32 Hz. For the PSWIB with triangular arrangement, the frequency range of the first complete band gap for the x and y mode is 64 Hz–102 Hz, with a gap width of 38 Hz.

Compared to conventional WIB, the PSWIB exhibits significantly improved vibration isolation frequency and bandwidth, leading to enhanced vibration control performance. Furthermore, when the PSWIB is arranged in a triangular configuration, a wider frequency range of band gaps can be achieved, resulting in stronger vibration isolation performance. Therefore, for practical engineering applications, the triangular arrangement form should be considered as the preferred option. It is worth mentioning that this investigation exclusively concentrated on the band gaps pertaining to the x and y modes, whereas the band gaps of the z mode could be explored using a commensurate approach.

3 Bandgap analysis by finite element method

In this study, the band gaps of the PSWIB in square and triangular arrangements were initially computed using the plane wave expansion method, resulting in wide vibration isolation frequency bands. To compare the obtained band gap results with theoretical calculations, the vibration isolation performance was analyzed using the COMSOL finite element software in this section (Hsu and Wu, 2007). Figure 5 illustrates the unit cell models of the PSWIB in square and triangular arrangements, with identical dimensions and material parameters consistent with Table 1.

The solid mechanics characteristic frequency module of the COMSOL finite element software was employed to perform the calculations. The model was configured with Floquet periodic boundary conditions in the x and y directions, while the

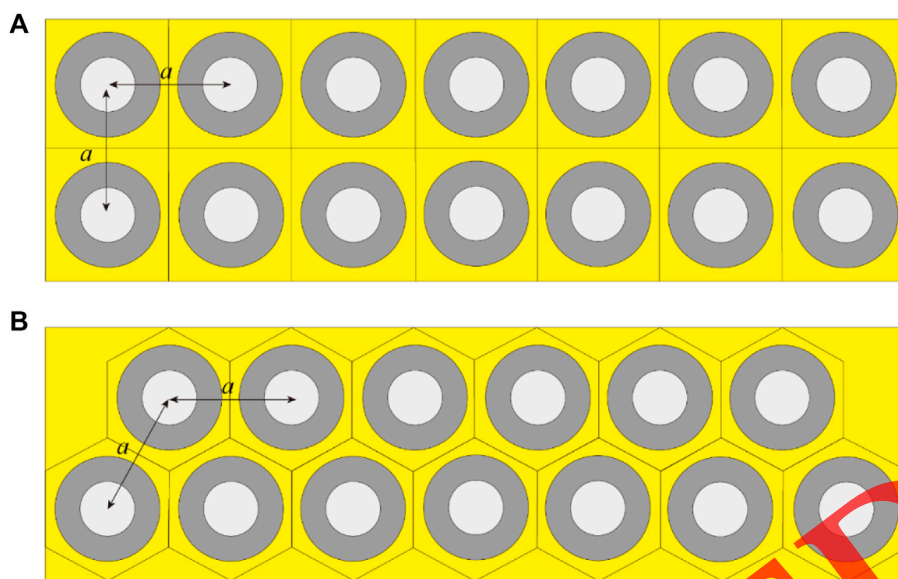


FIGURE 1
PSWIB schematic diagram. (A) square arrangement, (B) triangular arrangement.

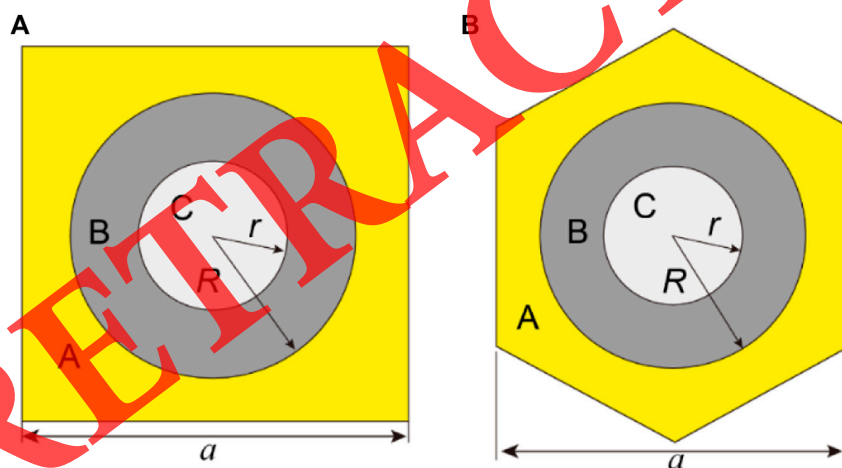


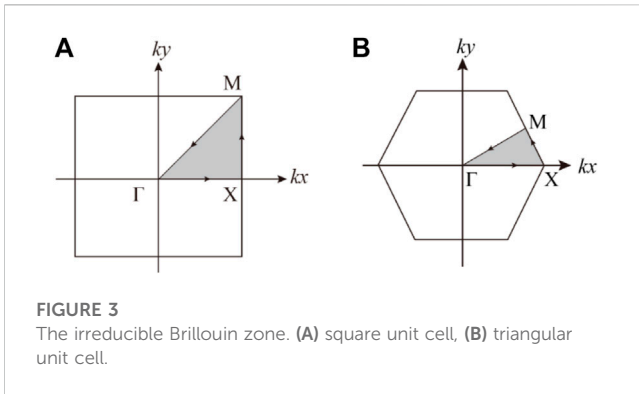
FIGURE 2
Cell structure of periodic wave impeding block. (A) square unit cell, (B) triangular unit cell.

TABLE 1 Elastic material parameters.

Material	Density ρ (kg/m ³)	Young modulus E ($\times 10^6$ Pa)	Poisson ratio ν
Concrete	2,300	30,000	0.2
Silicon rubber	1,300	0.1175	0.469
Silty clay	2023	0.289	0.313

parameterized scan involved selecting wave vectors, k , at the three high-symmetry points of the irreducible Brillouin zone. The band gap results obtained from the finite element software are presented in Figure 6,

where the wave vector ranges on the x -axis, namely, 0–1, 1–2, and 2–3, correspond to the wave vector ranges M– Γ , Γ –X, and X–M, respectively, in the theoretically calculated band gap diagram shown in Figure 4.

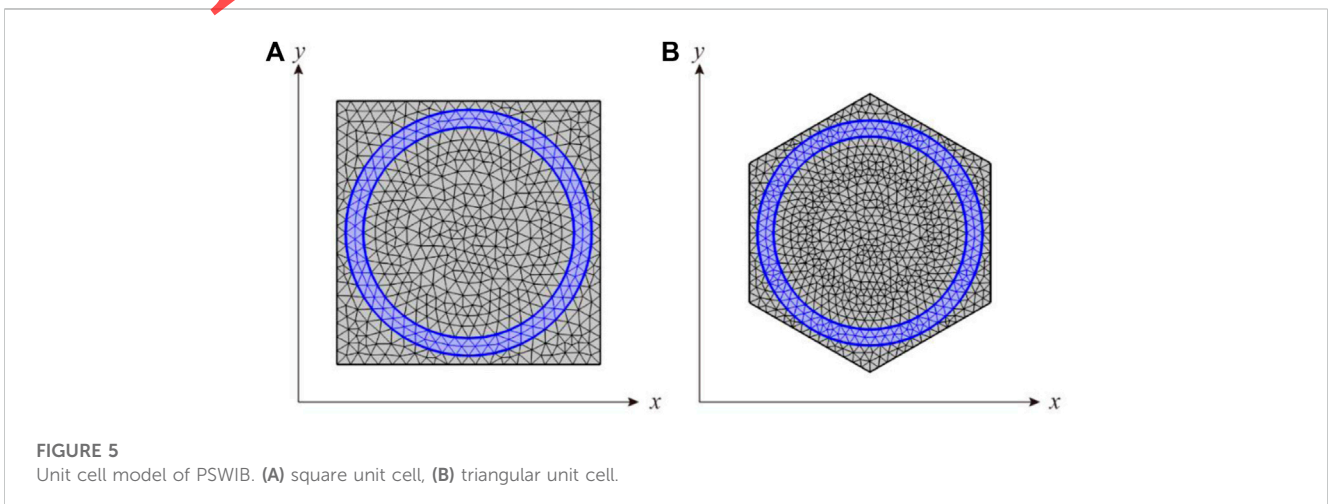
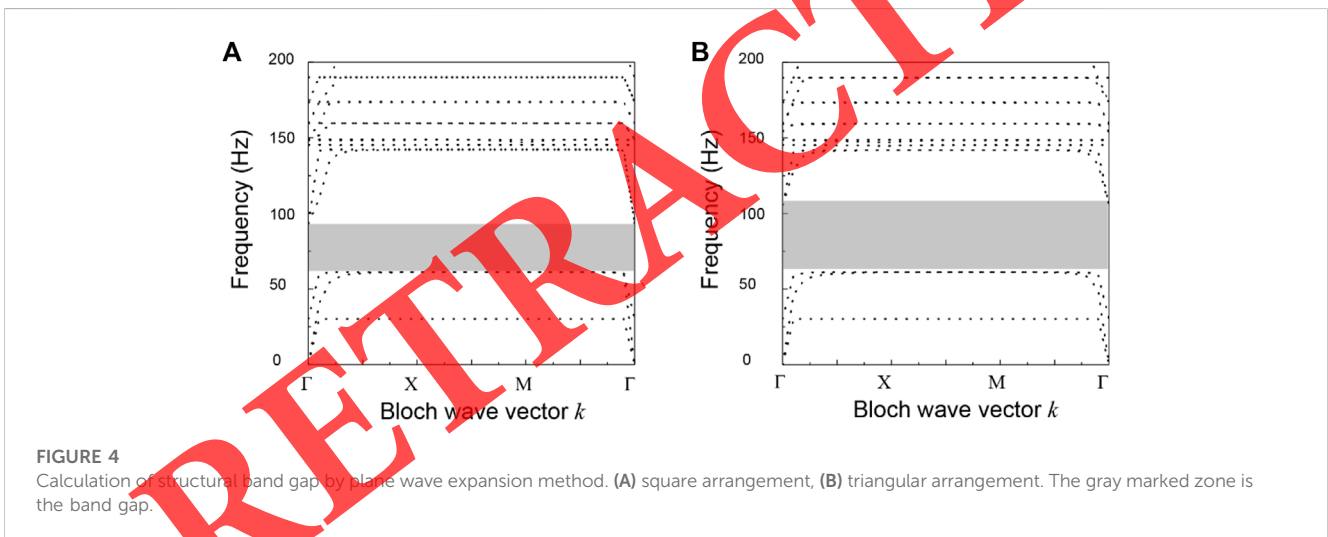


The band gap frequencies obtained from the COMSOL finite element method are shown in Figures 6A, B. In the case of the square arrangement, the computed band gap frequency range is 61–92 Hz, with a width of 31 Hz. For the triangular arrangement, the computed band gap frequency range is 61–105 Hz, with a width of 44 Hz. A comparison between the theoretically calculated band gap results

from the plane wave expansion method (Figures 4A, B) and the numerical simulation results reveals a close match in the frequency range of the band gaps, with small errors and good agreement. Furthermore, for the square arrangement, the repetition region of the first complete band gap in the x and y mode spans from 61 Hz to 92 Hz, while for the triangular arrangement, the repetition region of the first complete band gap in the x and y mode spans from 64 Hz to 102 Hz. These correspond to band gap ranges that can provide complete suppression of elastic waves.

4 Analysis of frequency response curve of finite PSWIB

The band gap positions and widths in infinite periodic structures can be achieved through theoretical calculations and finite element software. However, in practical engineering applications, periodic structures exhibit finite periodicity rather than infinite periodicity. To evaluate the band gap characteristics of finite PSWIB, the attenuation effects were investigated using the frequency response function based on the COMSOL finite element solid mechanics



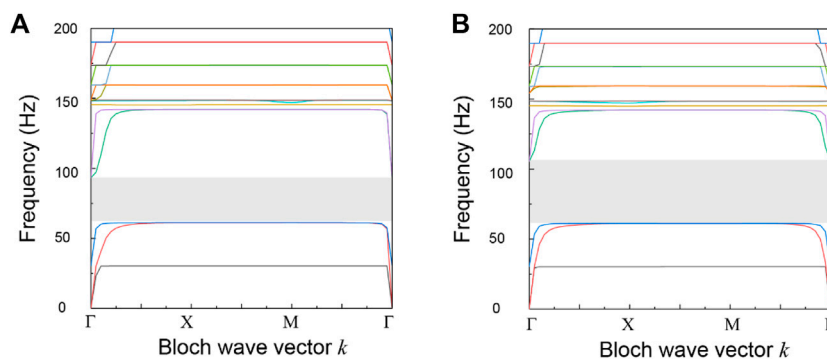


FIGURE 6

Calculation of structural bandgap by finite element. (A) square arrangement, (B) triangular arrangement. The gray marked zone is the bandgap.

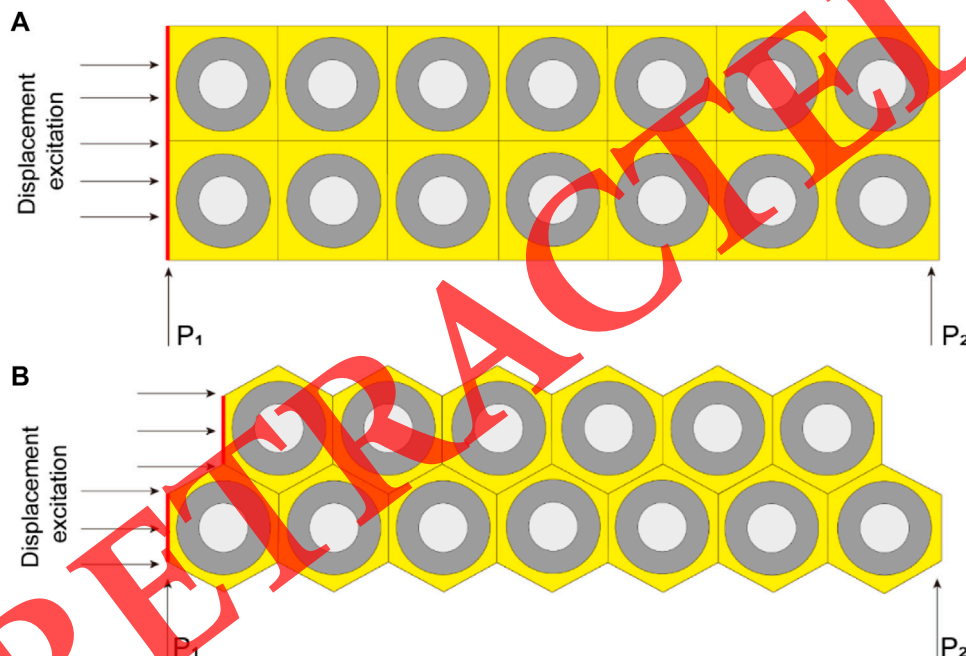


FIGURE 7

Transmission model of finite PSWIB. (A) square arrangement, (B) triangular arrangement.

frequency domain module. Figures 7A, B depict the models of finite PSWIB arranged in square and triangular configurations, respectively. The structural parameters and material attributes of these models mirror those of infinite PSWIB, with no consideration of any impact from additional structural mass.

Unit displacement excitations in the specified y -direction were applied to one side of the models, while domain point probes were positioned at P1 and P2 to measure the input and output displacements, respectively. To ensure accurate computations, a step size of 0.05 Hz was employed, scanning from 1 Hz to 160 Hz. The frequency response function was defined as follows (Hsu and Wu, 2007):

$$TL = 20 \log_{10} \frac{|ppb2|}{|ppb1|}, \quad (11)$$

where TL represents the value of the frequency response function, ppb2 denotes the output displacement response, and ppb1 represents the input displacement excitation.

Figures 8A, B depict the frequency response curves for the square and triangular arrangements, respectively. Since bandgaps can impede the propagation of elastic waves, the frequency response curves can intuitively reflect the attenuation ability of bandgaps on elastic wave propagation. Within the frequency range of 1–160 Hz, the frequency response values corresponding to the bandgap range should be significantly smaller than 1. The shaded region in Figure 8 represents substantial vibration attenuation, which corresponds to the bandgap. For Figure 8A, the frequency range of vibration attenuation is 61–91 Hz, with a maximum amplitude attenuation of 47 dB within the attenuation region. For Figure 8B, the frequency

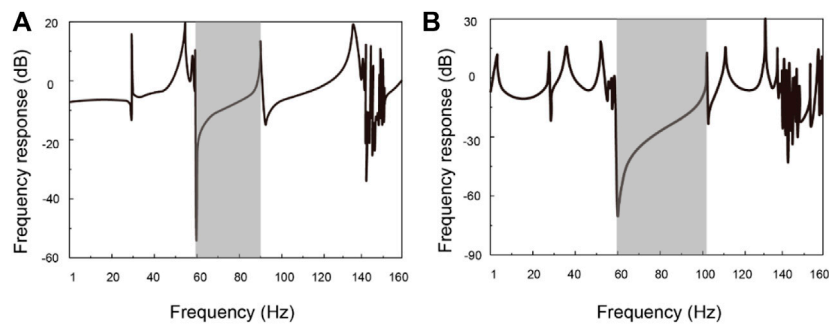


FIGURE 8

Frequency response curve of PSWIB. (A) square arrangement, (B) triangular arrangement. The gray marked zone is the band gap.

range of vibration attenuation is 61–105 Hz, with a maximum amplitude attenuation of 65 dB within the attenuation region. While some level of vibration amplification occurs in other frequency ranges, the vibration attenuation region efficiently controls and isolates elastic wave propagation, thereby achieving vibration isolation for the target frequency within the attenuation area. Compared to the square arrangement, the triangular arrangement exhibits a wider range of vibration attenuation and a stronger suppression effect on the propagation of elastic waves. Moreover, the consistency between the frequency attenuation range of the finite PSWIB and the bandgap diagram in Figure 4 of the ideal infinite structure is good, which once again verifies the correctness and reliability of the bandgap in the infinite PSWIB.

Based on the above research, it can be concluded that the PSWIB has its inherent vibration isolation advantages and relies on the structural bandgap for vibration control. The bandgap range is wide, and the maximum attenuation within the vibration attenuation region is significant. Moreover, it no longer relies on the cut-off frequency of the foundation for vibration isolation, thus breaking free from the dependence on cut-off frequencies that traditional WIB are constrained.

5 Analysis of factors influencing the bandgap of PSWIB

The parameters analyzed and studied include the periodic constant a , the inner radius of the cladding r , the outer radius of the cladding R , the number of structures in each layer, and the number of layers in the arrangement. The COMSOL, a finite element software, was used to calculate the structure bandgaps under different parameters. The starting frequency, cut-off frequency, and width of the bandgaps were summarized. The influence of the aforementioned parameters on the vibration attenuation region of the finite PSWIB was investigated using frequency response functions. In the course of varying a single parameter, all other variables were held constant, facilitating the isolation of the impact of the aforementioned parameters solely on the attributes of the first complete bandgap within the finite PSWIB, considering the triangular arrangement.

The effect of different periodic constants a on the bandgap characteristics of the PSWIB was studied. By varying the periodic constant a and taking values of 0.3, 0.35, 0.4, and 0.45 m, it can be observed from Figure 9A that the starting frequency remains unaffected, but the cut-off frequency gradually decreases and the bandgap width narrows as the periodic constant a increases. From the frequency response curve in Figure 9B, it can be observed that as the periodic constant a increases, the maximum attenuation amplitude in the vibration attenuation region increases from 65 to 84 dB. However, the range of the vibration attenuation region gradually decreases, indicating a weakened vibration isolation and attenuation capability. As such, to enhance the efficacy of vibration control in the periodic structure, opting for a smaller a is recommended.

The influence of different outer radii R of the coating layer on the PSWIB is discussed. The R was adjusted with values of 0.125, 0.13, 0.135, and 0.140 m. Figure 10A presents the relationship between the first complete bandgap and R , while Figure 10B illustrates the relationship between the frequency response curve and R . From Figure 10A, it can be observed that as R increases, the starting frequency, cutoff frequency, and bandgap width decrease simultaneously. In Figure 10B, the frequency response curve reveals that as R increases, the maximum amplitude attenuation within the vibration attenuation region of the PSWIB decreases from 80 to 65 dB. Additionally, the range of vibration attenuation also gradually reduces. Therefore, minimizing R should be considered to enhance the vibration isolation and attenuation performance.

The influence of different inner radii of the coating layer r on the PSWIB is investigated. The r was adjusted with values of 0.10, 0.11, 0.12, and 0.13 m. As shown in Figure 11A, it can be observed that with an increase in r , the starting frequency, cutoff frequency, and bandgap width simultaneously increase. In Figure 11B, the frequency response curve reveals that as r is progressively raised, the maximum amplitude attenuation within the vibration attenuation region of the PSWIB remains relatively stable, at around 65 dB. However, the coverage range of the vibration attenuation region gradually expands, thereby enhancing the vibration isolation and attenuation effectiveness. Therefore, selecting a larger r is beneficial for improving the vibration isolation and attenuation range of the PSWIB, thereby enhancing its vibration isolation performance.

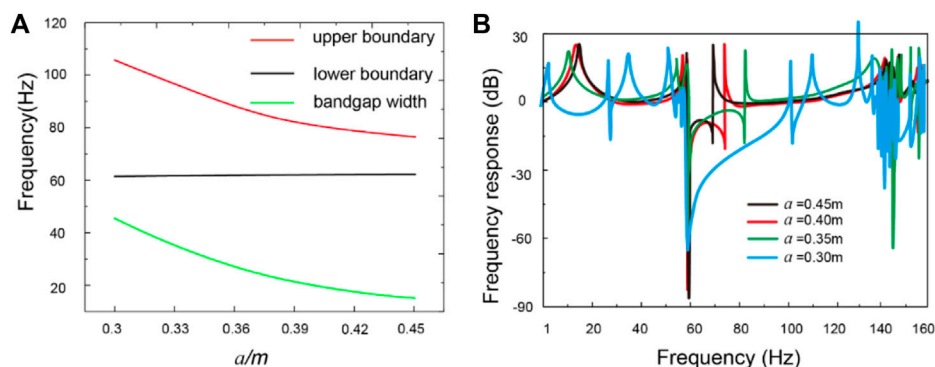


FIGURE 9

Influence of periodic constant a on PSWIB. (A) the relationship between the first complete bandgap and the periodic constant a , (B) the relationship between the frequency response curve and the periodic constant a .

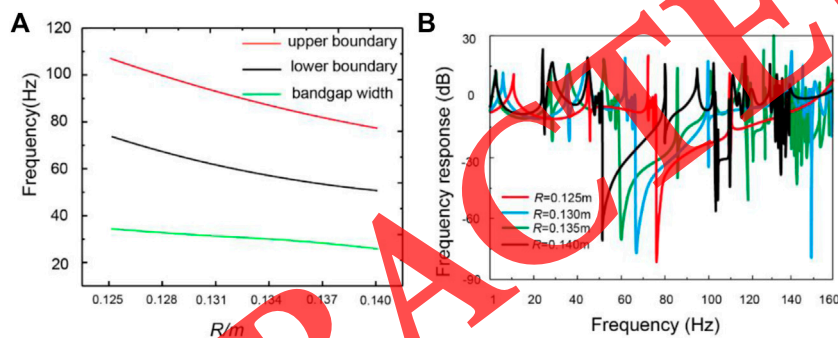


FIGURE 10

Influence of outer radii R of the coating layer on bandgap and frequency response of the PSWIB. (A) the relationship between the first complete bandgap and R , (B) the relationship between the frequency response curve and R .

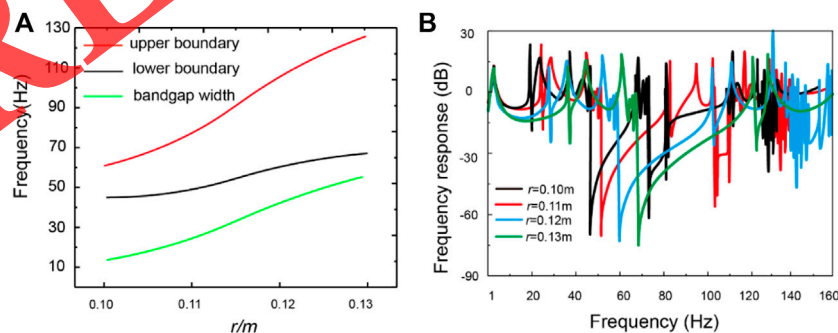


FIGURE 11

Influence of inner radii of cladding layer r on PSWIB. (A) the relationship between the first complete bandgap and r (B) the relationship between the frequency response curve and r .

The relationship between the frequency response curve of the finite PSWIB and the number of structures per layer is investigated. Since calculating a single structural unit is sufficient to determine the entire bandgap of the periodic structure, and the bandgap range remains consistent without altering the structural and material

parameters, this section does not discuss the variation pattern of the first complete bandgap. Instead, it focuses solely on analyzing the influence of the number of structures per layer on the frequency response curve. The study examines periodic structures with 2×4 cycles, 2×6 cycles, and 2×8 cycles, where 2 represents the number

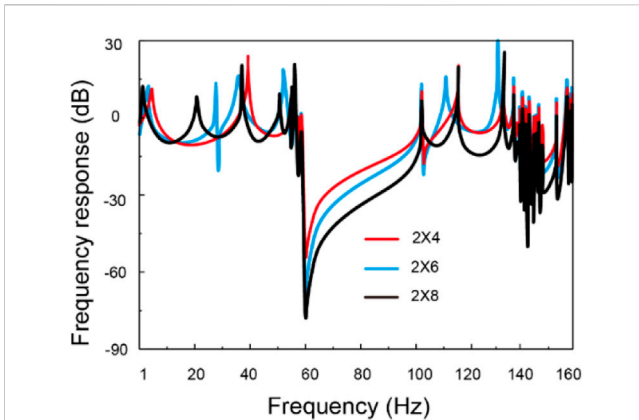


FIGURE 12
Influence of the number of periodic structure unit cell in each layer on the frequency response curve of PSWIB.

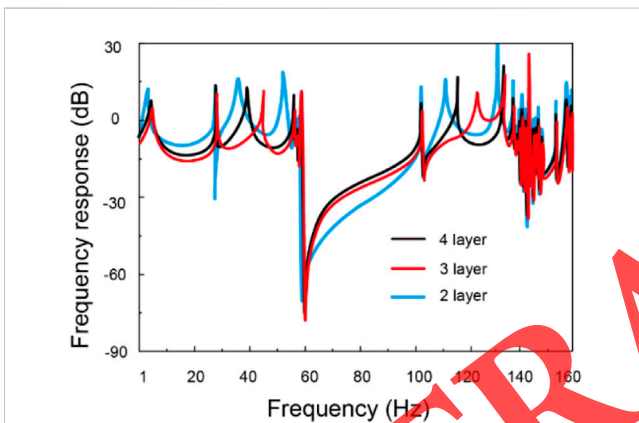


FIGURE 13
Influence of the number of layers on the frequency response curve of PSWIB.

of layers, and 4, 6, and 8 represent the number of structures per layer. As depicted in Figure 12, the maximum attenuation amplitude within the vibration attenuation region is 48 dB for the 2×4 cycle structure, 65 dB for the 2×6 cycle structure, and 74 dB for the 2×8 cycle structure. Choosing different numbers of structures does not affect the range of the vibration attenuation region of the PSWIB, but it progressively increases the maximum attenuation amplitude within that region. Thus, within a specific range, augmenting the number of structures per layer contributes to the enhancement of the vibration isolation efficacy of the PSWIB.

The influence of the number of layers in the arrangement of WIB on the vibration attenuation region of PSWIB is investigated. While keeping the number of structures per layer constant and not discussing the variation pattern of the bandgap, the number of layers in the PSWIB is sequentially set to 2 layers, 3 layers, and 4 layers. As shown in Figure 13, the maximum attenuation amplitude within the vibration attenuation region is 65 dB for the 2-layer periodic structure, 73 dB for the 3-layer periodic structure, and 80 dB for the 4-layer periodic structure. For different numbers of layers, the range of the vibration

attenuation region of the PSWIB remains consistent, staying around 61–105 Hz. However, the maximum attenuation amplitude within the vibration attenuation region gradually increases. Therefore, within a certain range, increasing the number of layers in the arrangement contributes to improving the vibration isolation performance of the PSWIB.

The aforementioned research indicates that rational design of the constituent parameters of PSWIBs can increase the magnitude of the isolation frequency, expand the range of vibration control, and enhance vibration isolation performance. Furthermore, the unique bandgap selection characteristic of periodic structures allows for the design of bandgaps according to specific requirements, enabling the isolation of different target frequency sources. This capability is not possessed by traditional WIB or certain improved WIB.

6 Conclusion

Drawing upon the principles of phononic crystals, a PSWIB is proposed, and its bandgaps are solved using the plane wave expansion method and the finite element method. A finite PSWIB model is established, and the vibration attenuation zone is calculated using the frequency response function. The influence of parameters such as the periodic constant a and the arrangement shape on the bandgaps and attenuation zone of the PSWIB is discussed. To optimize the PSWIB, an orthogonal design approach is employed, linking critical factors shaping bandgap characteristics with an orthogonal experimental design pattern.

The main conclusions are as follows:

- (1) The results of theoretical calculations and numerical simulations show good consistency. Compared to traditional WIB, PSWIB, based on their unique bandgap characteristics, greatly increases the isolation frequency and bandwidth, and significantly enhance vibration control performance. Notably, within similar conditions, PSWIBs arranged in triangles offer superior performance in terms of vibration isolation and attenuation.
- (2) The vibration attenuation zone of the finite periodic structure is basically consistent with the bandgaps calculated for the infinite periodic structure, further verifying the correctness and reliability of the bandgaps of infinite PSWIB. Additionally, the vibration attenuation zone of PSWIB has a wider range and larger maximum attenuation amplitude. It no longer relies on the cut-off frequency of the soil layer for vibration isolation and attenuation, getting rid of the limitations of traditional WIB.
- (3) Rational design of the structural parameters of the PSWIB can achieve bandgaps that meet practical needs and control isolation for different target frequencies. Increasing the periodic constant, a keeps the starting frequency unchanged, but the cutoff frequency and bandgap width gradually decrease, while the maximum attenuation amplitude increases from 65 dB to 84 dB. Increasing the R results in a decrease in the starting frequency, cutoff frequency, bandgap width, and maximum vibration

attenuation amplitude, reducing the maximum attenuation amplitude from 80dB to 65 dB. Increasing the inner radius r of the cladding layer leads to an increase in the starting frequency, cutoff frequency, and bandgap width, while the maximum amplitude attenuation value remains almost the same, all around 65 dB. Increasing the number of layers and the number of structures per layer does not significantly affect the range of the vibration attenuation zone, but the maximum attenuation amplitude gradually increases.

Data availability statement

The raw data supporting the conclusion of this article will be made available by the authors, without undue reservation.

Author contributions

YL: Data curation, Methodology, Software, Writing—original draft. XZ: Conceptualization, Supervision, Writing—review and editing. LS: Funding acquisition, Project administration, Writing—original draft.

References

- Atalan, M., Prendergast, L. J., Grizi, A., and Thom, N. (2022). A review of numerical models for Slab-Asphalt track railways. *Infrastructures* 7 (4), 59. doi:10.3390/infrastructures7040059
- Çelebi, E., and Göktepe, F. (2012). Non-linear 2-D FE analysis for the assessment of isolation performance of wave impeding barrier in reduction of railway-induced surface waves. *Constr. Build. Mater.* 36, 1–13. doi:10.1016/j.conbuildmat.2012.04.054
- Chen, J., Geng, J., Gao, G., Luo, W., Liu, Y., and Li, K. (2022). Mitigation of subway-induced low-frequency vibrations using a wave impeding block. *Transp. Geotech.* 37, 100862. doi:10.1016/j.trgeo.2022.100862
- Chow, N., Le, R., and Schmid, G. (1991). Propagation of vibration in a soil layer over bedrock. *Eng. Anal. Bound. Elem.* 8 (3), 125–131. doi:10.1016/0955-7997(91)90021-K
- Gao, G., Chen, J., Gu, X., Song, J., and Li, S. (2017). Numerical study on the active vibration isolation by wave impeding block in saturated soils under vertical loading. *Soil Dyn. Earthq. Eng.* 93, 99–112. doi:10.1016/j.soildyn.2016.12.006
- Gao, G., Li, N., and Gu, X. (2015). Field experiment and numerical study on active vibration isolation by horizontal blocks in layered ground under vertical loading. *Soil Dyn. Earthq. Eng.* 69 (69), 251–261. doi:10.1016/j.soildyn.2014.11.006
- Hsu, J. C., and Wu, T. T. (2006). Efficient formulation for band-structure calculations of two-dimensional phononic-crystal plates. *Phys. Rev. B* 74 (14), 144303. doi:10.1103/PhysRevB.74.144303
- Hsu, J. C., and Wu, T. T. (2007). Lamb waves in binary locally resonant phononic plates with two-dimensional lattices. *Appl. Phys. Lett.* 90 (20). doi:10.1063/1.2739369
- Li, X., Chen, Y., Zou, C., and Chen, Y. (2023b). Train-induced vibration mitigation based on foundation improvement. *J. Build. Eng.* 76, 107106. doi:10.1016/j.jobbe.2023.107106
- Li, Z., Ma, M., Liu, K., and Jiang, B. (2023a). Performance of rubber-concrete composite periodic barriers applied in attenuating ground vibrations induced by metro trains. *Eng. Struct.* 285, 116027. doi:10.1016/j.engstruct.2023.116027
- Lombaert, G., Degrande, G., François, S., and Thompson, D. J. (2015). “Ground-borne vibration due to railway traffic: A review of excitation mechanisms, prediction methods and mitigation measures,” in *Noise and vibration mitigation for rail transportation systems: Proceedings of the 11th international workshop on railway noise, uddevalla, Sweden, 9–13 september 2013* (Germany: Springer Berlin Heidelberg), 253–287.
- Ma, Q., Shu, J., and Zhou, F. (2022). Theoretical study of S wave passing through a double-layer wave impeding block in the unsaturated soil. *Comput. Geotech.* 152, 105018. doi:10.1016/j.compgeo.2022.105018
- Ma, Q., Zhou, F. X., and Zhang, W. Y. (2019). Vibration isolation of saturated foundations by functionally graded wave impeding block under a moving load. *J. Braz. Soc. Mech.* 41, 108–110. doi:10.1007/s40430-019-1602-5
- Peplow, A. T., Jones, C. J. C., and Petyt, M. J. A. A. (1999). Surface vibration propagation over a layered elastic half-space with an inclusion. *Appl. Acoust.* 56 (4), 283–296. doi:10.1016/S0003-682X(98)00031-0
- Peplow, A. T., and Kaynia, A. M. (2007). Prediction and validation of traffic vibration reduction due to cement column stabilization. *Soil Dyn. Earthq. Eng.* 27 (8), 793–802. doi:10.1016/j.soildyn.2007.01.002
- Schmid, G., Chow, N., and Le, R. (1992). Shielding of structures from soil vibrations. Proceedings of soil dynamics and earthquake engineering V. *Comput. Mech. Publ.*, 651–662.
- Takemiya, H. (2004). Field vibration mitigation by honeycomb WIB for pile foundations of a high-speed train viaduct. *Soil Dyn. Earthq. Eng.* 24 (1), 69–87. doi:10.1016/j.soildyn.2003.07.005
- Takemiya, H., and Fujiwara, A. J. S. D. (1994). Wave propagation/impediment in a stratum and wave impeding block (WIB) measured for SSL response reduction. *Soil Dyn. Earthq. Eng.* 13 (1), 49–61. doi:10.1016/0267-7261(94)90041-8
- Takemiya, H., Hashimoto, M., and Shiraga, A. (2002). Construction of wave impeding barrier (WIB column) for mitigation of traffic induced ground vibration. *Soil Found.* 50 (9), 19–21.
- Takemiya, H. (2003). Simulation of track-ground vibrations due to a high-speed train: the case of X-2000 at ledsgard. *J. Sound. Vib.* 261 (3), 503–526. doi:10.1016/S0022-460X(02)01007-6
- Thompson, D. J., Jiang, J., Toward, M. G. R., Hussein, M. F. M., Dijckmans, A., Coulier, P., et al. (2015). Mitigation of railway-induced vibration by using subgrade stiffening. *Soil Dyn. Earthq. Eng.* 79, 89–103. doi:10.1016/j.soildyn.2015.09.005
- Yan, G., Zou, H. X., Wang, S., Zhao, L. C., Gao, Q. H., Tan, T., et al. (2020). Large stroke quasi-zero stiffness vibration isolator using three-link mechanism. *J. Sound. Vib.* 478, 115344. doi:10.1016/j.jsv.2020.115344

Funding

The author(s) declare financial support was received for the research, authorship, and/or publication of this article. This work was supported by the Key research and development project of Jiangsu Province, (No. 2021GJZPY15); Gansu Provincial Science and Technology Commissioner Special (22CX8GA112).

Conflict of interest

The authors declare that the research was conducted in the absence of any commercial or financial relationships that could be construed as a potential conflict of interest.

Publisher's note

All claims expressed in this article are solely those of the authors and do not necessarily represent those of their affiliated organizations, or those of the publisher, the editors and the reviewers. Any product that may be evaluated in this article, or claim that may be made by its manufacturer, is not guaranteed or endorsed by the publisher.